Basic Principles in the Optical Design of Imaging Multiple Aperture Systems

E. M. Sabatke
Optical Sciences Center, University of Arizona
1630 East University Boulevard
Tucson, AZ 85721
erin.sabatke@optics.arizona.edu

J. H. Burge
Optical Sciences Center, University of Arizona
1630 East University Boulevard
Tucson, AZ 85721

ABSTRACT

We discuss the basic concepts that have been useful in our work designing multiple aperture telescopes with wide fields of view. We examine combining errors at zero field and errors that are linear as a function of field. An easy optimization for satisfying the sine condition to eliminate linear piston errors is given. Methods for estimating the RMS wavefront errors for the lower-order combining errors are given.

1 INTRODUCTION

The field of astronomy advances with the development of new and better telescopes and instruments. Larger telescopes give both better resolution and higher sensitivity, allowing observations of fainter objects in greater detail. Both on the ground and in space, single-mirror technologies have reached their limits, and multiple aperture systems are needed for gains in sensitivity and resolution.

On the ground, older telescopes use primaries made out of single, solid pieces of glass. This technology cannot be scaled up to mirror diameters larger than four meters or so. The weight of the glass causes the surface shape to deform as the mirror is tilted, and the massive mirror takes many hours to reach the thermal equilibrium needed for observing. Newer single glass primaries use rigid backing structures behind thinner glass facesheets, reducing the weight and the time to reach thermal equilibrium. Even this technology, though, cannot be scaled up indefinitely. There is a limit to how rigid a backing structure can be made and still have a lower mass than solid glass.

Larger telescopes, then, must be multiple aperture systems that use several large primary mirrors acting as a single system. The first generation of large, multiple aperture systems is now being built: the Keck telescope in Hawaii, the Very Large Telescope in Chile, the Large Binocular Telescope in Arizona, and others.

In space, the current technology of single-segment primaries has also reached its limit. Rocket shrouds limit

International Optical Design Conference 2002, Paul K. Manhart, José M. Sasián, Editors,
Proceedings of SPIE Vol. 4832 (2002) © 2002 SPIE · 0277-786X/02/$15.00

the size of mirrors that can be launched to about six meters in diameter. In addition, the weight of glass mirrors makes launches expensive. Future space telescopes must have larger collecting areas and lower weights. Multiple aperture systems can achieve these goals. Arrays of smaller mirrors that fit into current rocket shrouds can reach very high resolutions or can reach very large collecting areas if mounted close together. Also, the small segments can use new and lighter mirror technologies.

Since multiple aperture systems are becoming more common and designers for them are needed, an introductory paper will be useful. Many good studies in beam combining exist, beginning with Meinel in 1970.[1] However, there is not a good introductory paper aimed at lens designers without experience in the field of multiple aperture system design. This paper will provide an introduction to the design of imaging interferometers.

1.1 Imaging versus fringe interferometry

Imaging multiple aperture systems are fundamentally different than interferometers that measure fringe visibility and carry out astrometry. Imaging interferometers produce a real image over a wide field of view. The interferometric fringes are superimposed on the image, giving a higher resolution than with the individual mirrors alone.

Fringe interferometers, however, don't produce a real image. They instead measure fringe visibility as the mirrors' baselines are changed. They have a field of view of zero, and it would be very difficult to change the baselines drastically as well as maintain the conditions in the field required to produce an image. Also, many do not use adaptive optics to correct for the atmosphere. This means that the mirrors used are quite small, even compared to traditional imaging telescopes. The Keck interferometer and the VLT are the first large interferometers of this type to use adaptive optics, and they have very large primary mirrors.

Imaging interferometry has a strong history at the University of Arizona. The Multiple Mirror Telescope on Mt. Hopkins was the first telescope to carry out coherent beam combining, or imaging interferometry.[2] Coherent imaging in the MMT was difficult to maintain and required a skilled operator. The next generation of this technology is the Large Binocular Telescope,[3] currently being built on Mt. Graham. The LBT has an adaptive secondary and some tip/tilt/piston control in its other optics. This will allow easier coherent beam combining than the MMT, maintained by computer control. In addition, with the 20/20 telescope, the next generation of imaging interferometers is in the proposal stages.

2 INITIAL STEPS

2.1 Pixel sizes -> focal ratio

The focal ratio of a multiple aperture system is determined by the pixel sizes of the detector, just as it is in a single telescope. Images must be sampled at the Nyquist limit. This sets the f/# of the telescope. Often, the field of view is constrained by the detector as well, since detectors of larger size are very expensive.

2.2 Sensitivity and resolution -> Collection area and baseline

Knowledge of the detector array noise, other noise sources, and the magnitude of the science objects leads to a sensitivity requirement. This specifies the total collection area the telescope primary needs to have. In addition, the science objects will lead to a resolution requirement for the telescope. The resolution of an imaging

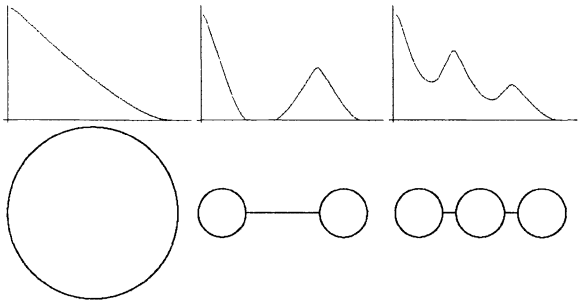

Figure 1: Pupil configurations are shown below their respective MTFs. The MTFs shown are cross-sections of half of the full MTF.

interferometer is given by its maximum baseline length, and is identical to the resolution calculation for a single telescope with the baseline length replacing the primary diameter. The angular resolution is: $\theta = \frac{2.44 \cdot \lambda}{B_{\max}}$, where $B_{\max}$ is the longest baseline of the system.

The ratio of total collection area to $\pi(B_{\max}/2)^2$ is often called the fill factor. A single telescope has a fill factor of one. A low fill factor implies apertures that are small compared to the maximum baseline, or a sparse array.

2.3 MTF details -> Array geometry

The sensitivity and resolution requirements don't place any constraints on the number of apertures or the specific positions of those apertures. The coverage of spatial frequencies needed will determine the specific array configuration. The modulus transfer function (MTF) is a plot of transmission efficiency versus spatial frequency. The science purposes of the telescope will determine how good the MTF must be. An astronomer may want to examine a known object in higher detail, or search for a predicted effect, and can use a narrow range of spatial frequencies. Surveillance satellites may not have a specific object to observe, and will need good coverage of a wide range of spatial frequencies.

In general, if the number of baselines of differing lengths is large, the coverage of spatial frequency space will be high. A system of two apertures samples one higher spatial frequency very well, as shown in Figure 1, but doesn't have the coverage that a single aperture of that diameter has. In general, the peak in the MTF due to a given baseline length, B, will be $B/(\lambda \cdot f)$ where f is the focal length of the system and λ is the wavelength. A system of three apertures can be thought of as three independent two-aperture systems, and the MTF of such a system will have three peaks at different frequencies if each of those baselines is a different length. If the three apertures are equally spaced, there are three baselines, but two have the same length. The MTF at the frequency corresponding to the repeated baseline will be higher. These ideas can be expanded to any number of apertures. There are several good papers in radio astronomy that calculate the configurations with the highest spatial frequency coverage for a given number of apertures.[4]

For a complicated array, calculating the frequency for each baseline is tedious. It is easier to use a plotting trick to locate the peaks of the MTF. The MTF in a linear system is proportional to the autocorrelation of the pupil function, and an autocorrelation is a shift-and-multiply function.[5] If the center of each aperture is marked, it creates an array of points. If another identical ray is shifted around the first, and the positions of each point marked when any two points of the arrays overlap, the result is a scaled plot of the peak frequencies in the MTF. Dividing the spatial coordinates by $(\lambda \cdot f)$ plots the MTF peaks to their proper frequencies. Figure 2 shows the

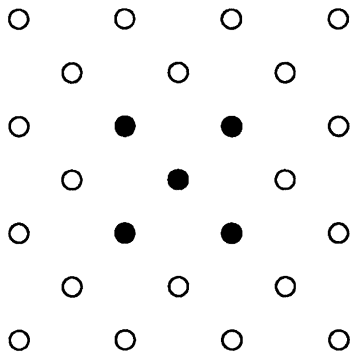

Figure 2: A plot of the peaks in the MTF for an array of five apertures.

process and the resulting MTF peaks. The locations of the original five apertures are shown with black dots. The empty dots show the positions of the elements in a second array, as it is shifted around the first array so that every element overlaps once with every element in the original array.

2.4 Geometry for the arms

With the primary configuration settled, the beam combining elements must be chosen. This procedure is very familiar to lens designers. It is best to choose as simple a geometry as possible, and begin with as few mirrors as possible. If the simplest configuration cannot achieve the field of view that is needed, additional mirrors can be added later. The size and the cost of the system must influence these choices, and it may not be possible to reach the requested field of view for the amount of money available.

3 PHYSICAL PICTURE OF BEAM COMBINING

We have found that a mental picture of the perfect image from two apertures has been very useful in our design work. The image intensity of a general two aperture system, free of all aberrations, is:

$$I(\xi,\eta) = D_1^2 \cdot Somb^2(D_1\rho) + D_2^2 \cdot Somb^2(D_2\rho) + 2 \cdot D_1 \cdot D_2 \cdot Somb^2(D_1\rho) \cdot Somb^2(D_2\rho) \cdot \cos[2\pi(x_1 - x_2)\xi + 2\pi(y_1 - y_2)\eta] \quad (1)$$

where $Somb(r) = \frac{2J_1(r)}{r}$ and J_1 is the first order Bessel function of the first kind. The variable $\rho = \sqrt{\xi^2 + \eta^2}$, and is a coordinate in spatial frequency space. The parameters $D_1$and D_2 are the diameters of the two circular apertures, and $\{x_1, y_1\}, \{x_2, y_2\}$ are the coordinates of the centers of the apertures in real space.

This image has three parts: an image from the first aperture, an image from the second aperture, and a set of cosine fringes under an envelope. (Notice that the frequency of the cosine fringes depends on the baseline separations.) For good images, then:

- the individual images from each aperture must overlap
- the combined images have to coincide with the center of the fringes

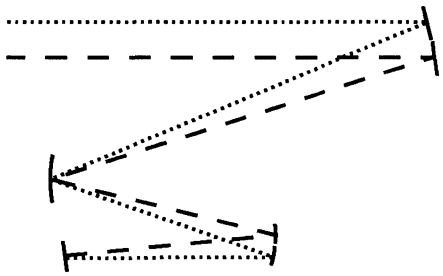

Figure 3: To align the fringe center with the individual images at zero field angle, the axial pathlengths in each arm must match.

- the images and fringes must stay together as the field angle changes
- the individual images must be well-corrected

4 CORRECTION OF COMBINING ERRORS

Assume for the moment that the individual images are perfect, so that the combining effects alone can be treated. First, the system must work well at a field angle of zero. Then, the first order errors that are linear as a function of field must be eliminated: linear tilt errors, linear power errors, and linear piston errors. Then, errors of a higher order in field can be eliminated if there are any remaining degrees of freedom.

4.1 Corrections at Zero Field Angle

There are only two issues to consider when the field angle is at zero. The first is the requirement that the individual images should overlap. This sets the pointing of the telescope.

The second requirement is that the images must overlap with the fringe centers. The fringe center is located where the pathlengths for the axial rays in the arms match, as shown in Figure 3. For each wavelength of optical path difference, the fringe center will shift by $\delta y = \frac{\alpha \lambda f}{B_y}$ and $\delta x = \frac{\alpha \lambda f}{B_x}$, where α is the optical path difference in waves, λ is the wavelength, and f is the focal length of the system, and B_y, B_x are baseline lengths in x and y, respectively. If the fringe center moves entirely off the geometric images, the resolution decreases to the Airy size of a single aperture. The Strehl drops to 0.5, because the individual images are adding only in intensity instead of amplitude, and would be twice as high if interference were occurring.

The RMS wavefront error for an optical path difference between arms of the interferometer can be calculated. This will be discussed in more detail under the section "Linear Piston Errors".

4.2 Linear Tilt Errors

Tilt errors can appear, independently in each aperture, that are linear as a function of field. These errors will cause the individual images to move apart. To first order, the images will move by $\delta y = \alpha \cdot f$ in each aperture for small field angles, where α is the field angle and f is the focal length of the branch producing that image. To

prevent the images from separating, then, the focal lengths of each arm of the interferometer must match.

It is useful to estimate the wavefront error due to all of these lower-order combining errors, since there may not be enough degrees of freedom to correct them all. The most damaging errors must be eliminated first.

For two interferometer arms with mismatched focal lengths, the maximum distance of separation, Δ, between the focal points in the system image plane must be:

$$\Delta = (f_2 - f_1) \cdot \alpha_{\max} \tag{2}$$

where $\alpha_{\max}$ is the maximum field angle, and f_1 and f_2 are the effective focal lengths of two arms. If we assume that all of this distance is due to a tilt error in one of the arms and think of the other arm as correct, then the magnitude of the tilt wavefront error at the edge of the pupil in waves can be calculated as:

$$W_{111} = \frac{D \cdot \alpha_{\max}}{2 \cdot \lambda} \frac{f_2 - f_1}{f_1} \tag{3}$$

where D is the aperture diameter and λ is the wavelength. This gives a wavefront error functional form of:

$$W_k = W_{111} \cdot \rho \cos\theta = \frac{D \cdot \alpha_{\max}}{2 \cdot \lambda} \frac{f_2 - f_1}{f_1} \rho \cos\theta. \tag{4}$$

where $\rho = \frac{r}{D}$ is the normalized pupil coordinate. The polar position $r \cdot \cos\theta$ specifies a given point in the pupil. The wavefronts W_k can be calculated for any number of apertures.

If there are many branches in the system with differing focal lengths, the RMS wavefront error, σ^2, for the whole system of apertures will be a sum weighted by the areas of each aperture, A_k:

$$\sigma^2 = \frac{\sum A_k \cdot \sigma_k^2}{\sum A_k} \tag{5}$$

where

$$\sigma_k^2 = \frac{1}{A_k} \iint_{A_k} (W_k - \langle W \rangle)^2 \delta A_k \tag{6}$$

and

$$\langle W \rangle = \frac{\sum A_k \langle W_k \rangle}{\sum A_k} \tag{7}$$

$$\langle W_k \rangle = \frac{\iint W_k \cdot \delta A_k}{A_k} \tag{8}$$

so that $\langle W \rangle$ is the weighted average of the wavefront over all of the apertures, and $\langle W_k \rangle$ is the weighted average of the wavefront over the kth aperture.

Finally, for small wavefront errors, the RMS wavefront error is related to the Strehl ratio by:

$$S = e^{-(2\pi \frac{\sigma}{\lambda})^2}. \tag{9}$$

In the case shown, σ^2 and S are the results at the edge of the field, $\alpha_{\max}$. These can also be plotted as a function of field angle, by allowing $\alpha_{\max}$ to vary, and evaluating the result at each field point. This could be important, since each error may dominate in only a finite region of field angle.

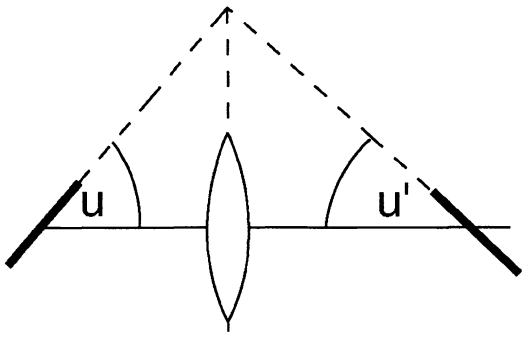

Figure 4: The Scheimpflug condition states that the object and image plane of an optical system must intersect at the principle plane(s).

4.3 Linear Power Errors

The image planes for each arm of the interferometer may be tilted with respect to one another. This leads to defocus errors that are linear as a function of field angle, since the distance between the system's image plane and the individual image plane increases linearly with distance away from the centers.

To first order, the image plane tilt can be calculated using the Scheimpflug condition.[6] The condition states that the object and image planes of an optical system will intersect at the principle planes of the system, as shown in Figure 4.

The image plane angle from the horizontal, u', can be calculated by tracing a ray that lies in the object plane. The output ray must lie in the image plane. Since the object plane tilt is often a small angle from the vertical, however, the ray angle, u, is usually large and far from paraxial. To first order:

$$u' = \frac{1}{n'} \cdot ArcTan[n \cdot Tan(u) - (y_o + z \cdot Tan(u))\phi] \tag{10}$$

where ϕ is the system power, n and n' are the indeces in object and image space, y_o is a vertical offset of the center of the object plane, and z is the horizontal distance from the object plane to the principle plane. For more complex systems, this calculation can be done for each element, with the image plane of the previous optic acting as the object plane for the following optic.

For an image plane tilted a small angle β from the system's image plane, the RMS wavefront error (and therefore the Strehl) as a function of field can be estimated. For an aperture near the system axis compared to the focal length, and at a small field angle $\alpha_{\max}$, the distance between the planes is:

$$\varepsilon_z = f \cdot \beta \cdot \alpha_{\max}. \tag{11}$$

The magnitude of the defocus error in waves, given the f/# of the tilted branch, is:

$$W_{020} = \frac{\varepsilon_z}{8(f/\#)^2 \cdot \lambda} \tag{12}$$

which gives a wavefront with the functional form:

$$W_k = W_{020} \cdot \rho^2 = \frac{f \cdot \beta \cdot \alpha_{\max}}{8(f/\#)^2 \cdot \lambda} \cdot \rho^2 \tag{13}$$

.

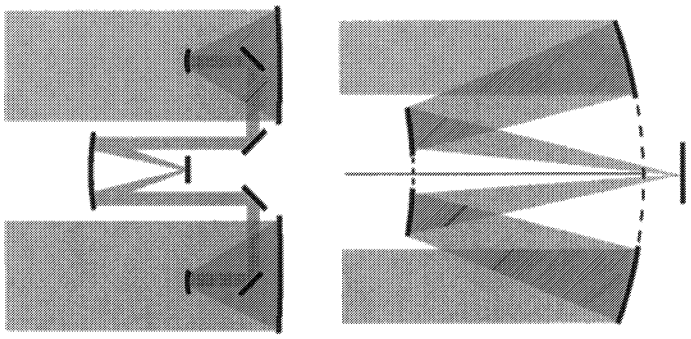

Figure 5: Afocal telescopes that share a single combining system also share a single focal plane. Systems that are off-axis sections of a single parent sytsem also have a single focal plane.

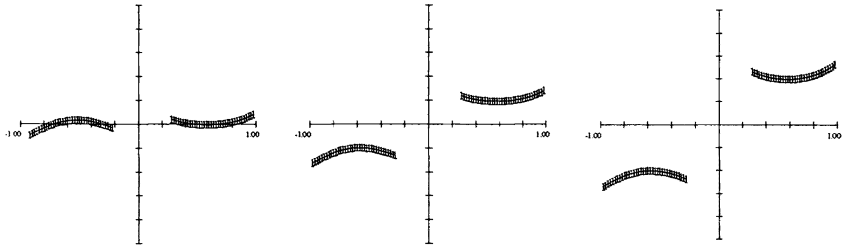

Figure 6: Wave fans from a two aperture system where linear piston error dominates. From left to right, the field angles are $\theta, 2\theta$, and 3θ. The piston error is obviously linear, roughly doubling with every doubling of field angle.

As discussed above, the total wavefront error for a system can be calculated using Equations 5,6, and 7. The RMS wavefront error due to linear power errors as a function of field can be calculated by allowing the value of $\alpha_{\max}$ to vary.

Given enough degrees of freedom, linear power errors can be corrected by design. Arrays of afocal telescopes that are combined with shared collection optics do not suffer from image plane tilts, because the optics are all axially symmetric and parallel to one another, and the fold flats are oriented at 45° (see Figure 5). Systems that are off-axis sections of axially symmetric systems also have no relative image plane tilts, since the parent system has a single focal plane. These two types of systems, however, are only a very small part of the possible design space for multiple aperture systems. It would be a mistake to rule out more general systems just to eliminate the relative image plane tilts. In a more general system, the image plane tilt can be controlled if the surface shape of at least one mirror is not axially symmetric.

4.4 Linear Piston Errors

Piston errors are mismatches in axial pathlength between individual arms of the interferometer. These errors cause the cosine fringes to move away from the individual images. Removing any constant piston error is easy, as discussed earlier, and just requires that the axial pathlengths in each arm match. This ensures that the centers of the apertures have no constant phase between them. With the constant piston term gone, piston error that is linear as a function of field should be corrected. Wave fans for a system with a dominant linear piston error are shown below.

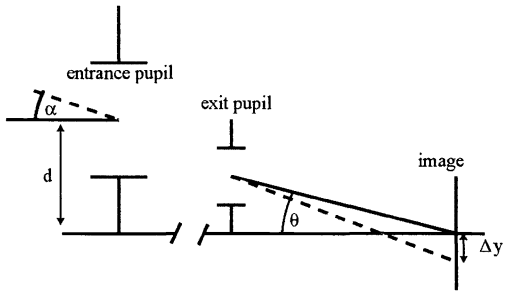

Figure 7: The locations of the individual images and the center of the fringes must coincide for small field angles.

If the axial path lengths as a function of field are known (analytically, or from real raytraces of the axial rays in each arm), the RMS wavefront error for the system can be very easily estimated. The functional form of the wavefront is just $W_k = W_{000} = \frac{\Delta}{\lambda}$, where Δ is the difference in optical path lengths between a given arm of the interferometer and a reference or perfect arm. The total wavefront error for a system can be calculated using Equations 5,6, and 7.

4.4.1 Correction of linear piston errors

Since piston errors cause the cosine fringes to move away from the individual images, we can correct the linear piston errors by demanding that the images and fringe centers stay together, to first order and for small angles. This can be done by satisfying:

$$\frac{d}{\sin\theta} = \frac{\Delta y}{\sin\alpha} \tag{14}$$

where the variables are defined in Figure 7, and α is a very small angle. The left side of the equation locates the fringe center, while the right side locates the individual images. Any additional arms of the interferometer must satisfy this same condition.

This method requires tracing only an axial ray and a ray at a small angle. Such rays are the least likely to be aberrated in a real system, making this correction method ideal for use in computerized optimization routines.

4.4.2 Relation to the Abbe sine condition

Correction of linear piston errors can also be achieved by satisfying the Abbe sine condition.

Lens designers are familiar with the Abbe sine condition as a way of eliminating coma. For a system with finite conjugates, the Abbe sine condition requires that the ratio of the input and output angles of a ray incident at angle u be equal to the magnification of the system, or $m = \frac{\sin u'}{\sin u}$. This must be satisfied everywhere in the pupil, or for all possible values of u. This is shown in Figure 8.

At first glance, this coma correction method seems unrelated to the correction of linear piston errors. The relationship is clear, though, if the entire wavefront of a multiple aperture system is considered. Figure 9 shows a two aperture system. If the entire wavefront had coma (W_{131}) in it, as shown, it would appear in the two apertures only as a piston error. The rest of the wavefront isn't sampled. For one aperture, the wavefront precedes the ideal in phase, and in the other aperture, the wavefront lags behind the ideal. Since coma is linear as a function of field, the piston error between the two apertures would also increase linearly as a function of field.

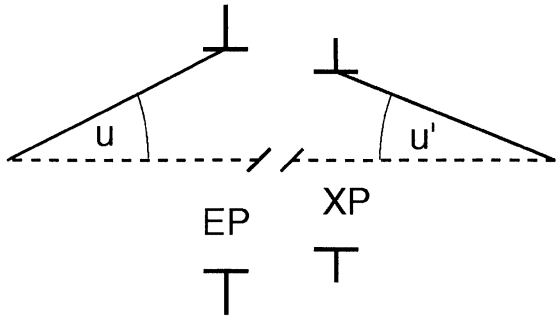

Figure 8: The Abbe sine condition requires that $sinu\prime/sinu = m$ everywhere in the pupil.

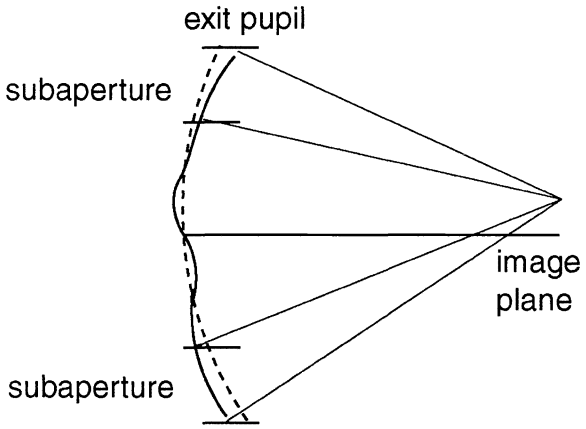

Figure 9: Linear piston error in a multiple aperture system can be viewed as due to system coma, and thus can be eliminated by satisfying the Abbe sine condition for the centers of the apertures.

Unlike coma correction, correcting linear piston errors does not require that the sine condition be satisfied everywhere in the pupil. If the sine condition is satisfied for the axial rays at zero field in each arm, the linear piston errors will be eliminated. The sine condition in the remaining parts of the aperture will be satisfied when the individual arm is corrected for coma, and can be ignored while working on the combining issues. This realization leads almost directly to Equation 14 and simplifies the optimization process. This understanding joins the physical understanding of piston error (shifting of cosine fringes) with the sine condition correction of the effect.

4.4.3 Relation to the "golden rule of separated telescopes"

For systems with an infinite conjugate, u=0, so the Abbe sine condition has the alternate form: $h = a \cdot \sin u'$. Since $a \cdot \sin u' = h'$, this is equivalent to saying that rays anywhere in the pupil must be scaled down equally (see Figure 8). So, this can be interpreted as a requirement that, in the absence of all other aberrations, the entrance and exit pupils of the system must be perfect, scaled copies of one another. For an afocal set of telescopes with a single combiner, this is even simpler: the diameters and separations of beams in image and object space must be differ only by a scaling factor. This has been called the "golden rule of separated telescopes".[7] It is a useful concept, since it is easy to flip a beam within a system in the early design stages without keeping this in mind.

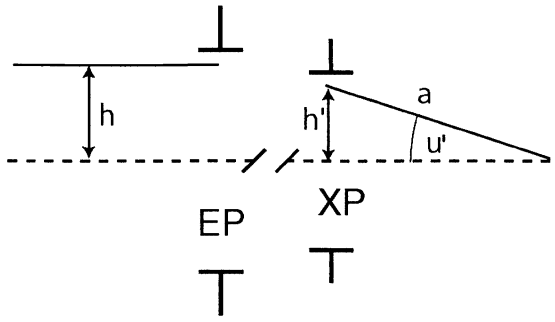

Figure 10: The sine condition has the form $h = a \cdot \sin\theta$ for systems with a finite conjugate.

However, it is less useful when optimizing a real system, since the rays that define the edges of the apertures in the entrance and exit pupils may be highly aberrated. In optimization, it is better to rely on Equation 14.

5 CORRECTION OF THE INDIVIDUAL ARMS

In general, each arm of the interferometer must be corrected for all third order aberrations. The arms of an interferometer may have only plane symmetry, so "third order aberrations" in this case includes some plane-symmetric aberrations that don't occur in the most standard axially symmetric systems.[8] Optimizing the individual arms is a familiar process for most lens designers, since it is almost equivalent to correction of any system with tilted and decentered elements. This can be done independently for each arm of the interferometer, without modelling the entire system. To do this, the beam combining requirements from above must be constrained so that they are not changed by the optimization routine:

- each arm must be optimized with respect to the system's image plane, rather than its preferred plane
- each arm must be constrained so that its focal length matches that of all the others
- each arm must satisfy the same sine condition as the others, for the zero-field axial ray

It is tempting to think that an equal amount of aberration in each arm might be better than a large mismatch in aberration values. This is especially true of aberrations that affect the position of the individual image, but not its quality, like field curvature and distortion. If the arms of a symmetric, two aperture system have equal amounts of distortion, then the individual images will be coincident with field. However, the final image is also includes the cosine fringes, not just the individual images. In the case of distortion, even though the individual images are coincident, the fringes may be elsewhere due to an OPD introduced by the distortion.

This is easy to see conceptually if the entire system wavefront is considered, as shown in Figure 11. Distortion at a single field angle looks like tilt. Each aperture is shown with the same amount of tilt. But what aberration has this introduced into the system as a whole? A guess at the entire wavefront is shown as a dashed line. It is a higher order aberration that will certainly degrade the image.

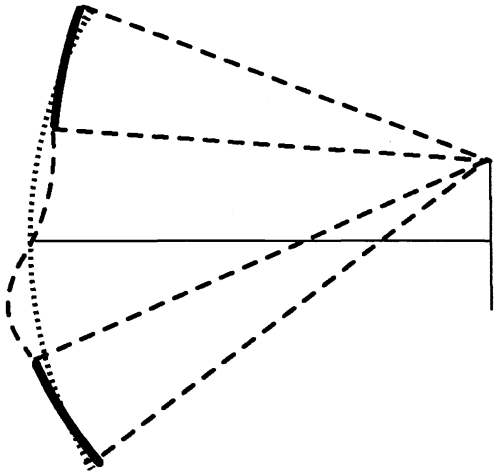

Figure 11: Equal amounts of distortion in each aperture correspond to a higher order aberration in terms of the system wavefront, which will degrade the image.

6 CONCLUSIONS

Multiple aperture system designers are needed, since the number of systems being built and proposed is increasing, both for space and ground-based applications. We have presented a practical overview of the optical design of a multiple aperture system. We have briefly covered the initial steps: establishing fill factors, baselines, and specific array geometries. We have discussed combining errors in more depth, including how they occur, how to estimate their effect on the system's performance, how to correct them, and in which order to attack them. Finally, we have pointed out the differences between correcting a general tilted and decentered system and correcting such a system for use in an interferometer.

7 REFERENCES

[1] A. B. Meinel, "Aperture Synthesis Using Independent Telescopes," *Applied Optics* **9**, no. 11 (November 1970): 2501-2504.

[2] E. K. Hege, J. M. Beckers, P.A. Strittmatter, D. W. McCarthy, "Multiple mirror telescope as a phased array telescope," *Applied Optics* **24**, no. 16 (15 August 1985): 2565-2576.

[3] J. M. Hill, Piero Salinari, "The Large Binocular Telescope Project" in *Telescope Structures Enclosures, Controls, Assembly/Integration/Validation, and Commissioning*, ed. T. A. Sebring, *Proceedings of SPIE* 4004 (March 2000): 36-46. Also see http://lbtwww.arcetri.astro.it/.

[4] M. J. E. Golay, "Point arrays having compact, nonredundant autocorrelations," *Journal of the Optical Society of America A* **62** (1971): 272-273.

[5] J. D. Gaskill, Linear Systems, "Convolutions" in *Linear Systems, Fourier Transforms, and Optics* (New York: John Wiley & Sons, 1978), 150-176.

[6] H. M. Merklinger, "Scheimpflug's Patent", Photo Techniques (Nov/Dec 1996).

[7] W. A. Traub, "Combining Beam From Separated Telescopes," *Applied Optics* **25**, no. 4 (15 February 1986): 528-532.

[8] J. M. Sasian, "How to approach the design of a bilateral symmetric optical system," *Optical Engineering* **33**, no. 6 (1994): 2045-2060.